Molecular Therapy
Original Article

Engineered clustered myoblast cell injection augments angiogenesis and muscle regeneration in peripheral artery disease

Keisuke Miyake, Shigeru Miyagawa, Akima Harada, and Yoshiki Sawa

Department of Cardiovascular Surgery, Osaka University Graduate School of Medicine, Osaka, Japan

The low survival rate of administered cells due to ischemic and inflammatory environments limits the efficacy of the current regenerative cell therapy in peripheral artery disease (PAD). This study aimed to develop a new method to enhance the efficacy of cell therapy in PAD using cell sheet technology. Clustered cells (CCs) from myoblast cell sheets obtained from C57/BL6 mice were administered into ischemic mouse muscles 7 days after induction of ischemia (defined as day 0). Control groups were administered with single myoblast cells (SCs) or saline. Cell survival, blood perfusion of the limb, angiogenesis, muscle regeneration, and inflammation status were evaluated. The survival of administered cells was markedly improved in CCs compared with SCs at days 7 and 28. CCs showed significantly improved blood perfusion, augmented angiogenesis with increased density of $CD31^+$/α-smooth muscle $actin^+$ arterioles, and accelerated muscle regeneration, along with the upregulation of associated genes. Additionally, inflammation status was well regulated by CCs administration. CCs administration increased the number of macrophages and then induced polarization into an anti-inflammatory phenotype ($CD11c^-$/$CD206^+$), along with the increased expression of genes associated with anti-inflammatory cytokines. Our findings suggest clinical potential of rescuing severely damaged limbs in PAD using CCs.

INTRODUCTION

The prevalence of peripheral artery disease (PAD) is increasing worldwide.[1] As the most severe form of PAD, chronic limb threatening ischemia (CLTI) is associated with an increased risk of major amputation rate and poor prognosis.[2] Surgical bypass and endovascular therapy are the mainstays of CLTI treatment; however, approximately 25% to 40% of CLTI patients are not eligible for revascularization because of the poor general and anatomical conditions.[3] For such patients, regenerative therapy, which induces angiogenesis to improve limb perfusion, is a good alternative to prevent major amputations. However, to date, there is no established regenerative therapy due to limited efficacy,[4–9] and current guidelines do not recommend regenerative therapy despite their potential therapeutic effects.[2,10] In particular, the low survival rate of administered cells in the ischemic and inflammatory environment of CLTI limits the efficacy of current regenerative cell therapy. Due to the low survival rate, the administered cells could not induce sufficient angiogenesis to change outcomes.[9,11]

In addition to enhancing angiogenesis in regenerative therapy in PAD, muscle regeneration should also be considered because recovering the ambulatory function is an important goal of CLTI treatment.[2] Deteriorated muscles due to poor blood supply lead to an impaired ambulatory function, an important predictor of poor prognosis.[12,13]

In myocardial ischemia, myoblast cell sheet implantation effectively restored cardiac function through angiogenesis induced by the paracrine effect of various cytokines.[14] In addition to the paracrine effect, the extracellular matrix (ECM) framework of cell sheets would have a beneficial effect for tissue regeneration.[15,16] The ECM plays an important role as an adhesive agent to the transplanted site and an anti-cell death agent, which would prevent early loss of administered cells, and also as a scaffold for angiogenesis.[16–18] However, cell sheet placement on ischemic leg muscles is not an ideal cell delivery method because of the large volume of ischemic muscles and the anatomical relationship between muscle surface and major arteries. Whereas coronary arteries are located on the surface of the heart, leg arteries are deep inside muscles. Considering that the administration of cells around occluded arteries is important to augment the arteriogenic process,[19] an injectable form of cells is more preferable than cell sheet placement in PAD because cell delivery into the perivascular area deep inside muscles is almost impossible to reach using cell sheets.

Therefore, using cell sheet technology, we developed novel injectable form clustered cells and investigated their efficacy on angiogenesis and muscle regeneration of ischemic limbs (see Figure 1 for the study protocol). We hypothesized that the injection of clustered cells with an ECM framework can augment cell survival and subsequently

Received 18 May 2021; accepted 5 January 2022;
https://doi.org/10.1016/j.ymthe.2022.01.008.

Correspondence: Yoshiki Sawa, Department of Cardiovascular Surgery, Osaka University Graduate School of Medicine, 2-2, Yamadaoka, Suita, Osaka 565-0871, Japan.
E-mail: sawa-p@surg1.med.osaka-u.ac.jp

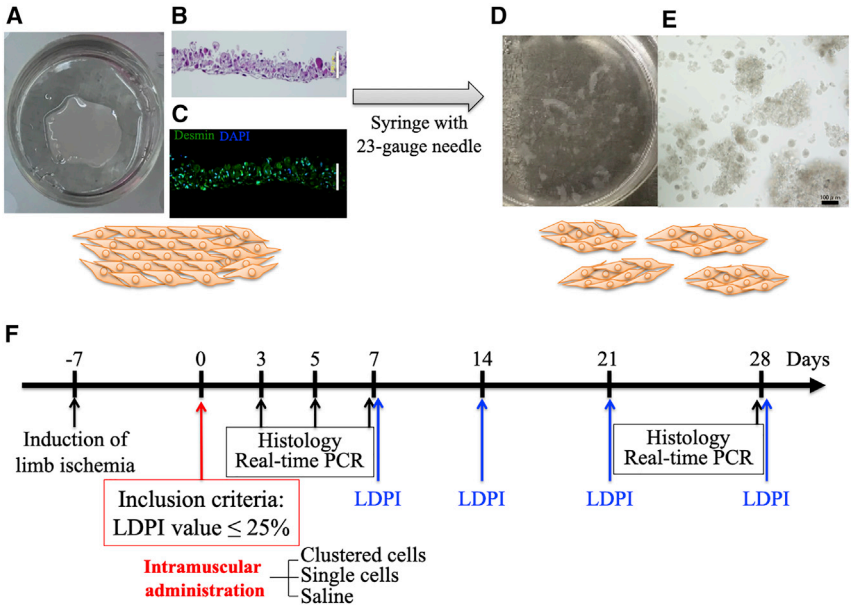

Figure 1. Creation of clustered cells and study protocol

(A) Cell sheet formation in a 12.8 mm temperature-responsive culture dish using 1.0×10^6 myoblast cells. (B) Representative images of H&E-stained cell sheets. (C) Immunohistochemical analysis of cell sheets. (D) Clustered cells on a dish. (E) Microscopic images of clustered cells. Scale bar: 100 μm. (F) Timeline of experimental protocol. RT-PCR, real-time PCR.

improve angiogenesis and tissue regeneration compared with single-cell administration.

RESULTS

Enhanced angiogenesis effect of clustered myoblast cells

Change in laser Doppler perfusion imaging value during time course

In this study, cells were administered into ischemic muscles 7 days after induction of hindlimb ischemia (defined as day 0). The time course of blood perfusion evaluated with laser Doppler perfusion imaging (LDPI) is shown in Figure 2. Compared with other groups, the clustered-cell group showed a marked improvement of blood perfusion early after administration (clustered cells, 41.8% ± 5.0%; single cells, 21.8%± 1.6%; and saline, 25.1% ± 3.4%, at day 7) and significantly improved perfusion status compared with other groups throughout the time course (clustered cells, 72.0% ± 3.2%; single cells, 49.0% ± 4.8%; and saline, 36.2% ± 3.2%, at day 28).

Density of microvasculature

The density of the microvasculature showed consistent results with blood perfusion changes. At day 28, the densities of the $CD31^+$ capillaries were 244.1 ± 34.7/mm^2, 201.6 ± 30.6/mm^2, and 109.1 ± 11.2/mm^2; and those of the $CD31^+/\alpha SMA^+$ arterioles were 71.7 ± 17.1/mm^2, 34.1 ± 3.1/mm^2, and 16.9 ± 3.2/mm^2 in the clustered-cell, single-cell, and saline groups, respectively (Figures 3A and 3B). Compared with the saline group, the clustered-cell group showed significantly higher numbers of both $CD31^+$ capillaries ($p = 0.009$) and $CD31^+/\alpha$-smooth muscle actin $(SMA)^+$ arterioles ($p = 0.005$). Although the number of $CD31^+$ capillaries was not significantly different between the clustered-cell and the single-cell groups ($p = 0.53$), the number of $CD31^+/\alpha SMA^+$ arterioles was significantly higher in the clustered-cell group ($p = 0.048$).

Expression of genes regarding angiogenesis

The expression of angiogenesis-related genes, including vascular endothelial growth factor (*VEGF*), hepatocyte growth factor (*HGF*), fibroblast growth factor 2 (*FGF2*), angiopoietin-1 (*ANGPT1*), and C-X-C motif chemokine ligand 12 (CXCL12), is shown in Figure 3C. The clustered-cell group showed higher values within 7 days after administration than other groups. The clustered-cell group, especially *VEGF* and *FGF2*, showed significantly higher values compared with the other two groups at day 5. At day 28, the expression of these angiogenesis-related factors was similar in all experimental groups.

Extracellular matrix formation and cell survival

ECM proteins, including fibronectin, laminin, and vitronectin, were well expressed in the clustered cells compared with single cells (Figures 4A and 4B). Laminin and fibronectin are mainly localized in the marginal areas of the cell cluster, whereas vitronectin is mainly found in the central area (Figure 4B). Significantly augmented cell survival was observed in the clustered-cell group compared with the single-cell group at days 7 (clustered cells, 2130.0 ± 554.5, and single cells, 471.4 ± 37.6; $p = 0.02$) and 28 (clustered cells, 411.8 ± 67.8, and single cells, 182.8 ± 17.9; $p = 0.008$) (Figures 4B and 4C).

Skeletal muscle regeneration

Enhanced skeletal muscle regenerative effect

Figure 5A shows the morphological change in ischemic skeletal muscles. At day 3, lysis of damaged muscle fibers was detected in the single-cell and saline groups but was seldom detected in the clustered-cell group. Cell infiltration into the temporary ECM, which is formed following tissue injury among muscle fibers and functions as a scaffold for tissue regeneration,[20] was detected, albeit at different degrees among the groups. At days 3 and 5, marked infiltration was detected in all groups. At day 7, a narrow interstitial space between muscle fibers was observed in the clustered-cell and single-cell groups, whereas a wide interstitial space between muscle fibers without marked cell infiltration was observed in the saline group. At day 28, in the clustered-cell group, almost normal alignments of muscle fibers with some cell infiltration were observed, whereas in the single-cell group, cell infiltration was still detected. In the saline group, the space remained wide with quite a few cell infiltrations detected in some areas.

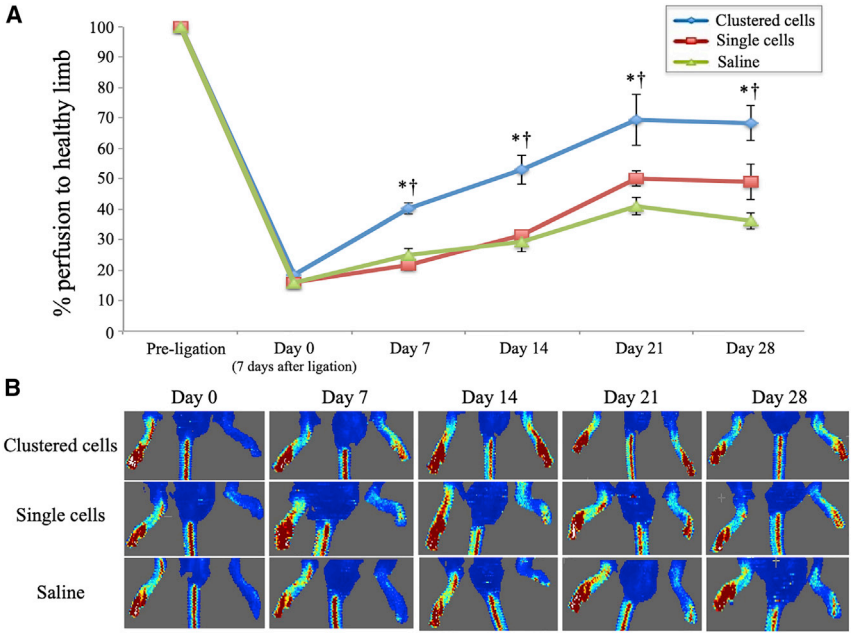

Figure 2. Time course change in limb perfusion

(A) Changes in hindlimb perfusion at pre-ligation (non-ischemic) and days 0 (7 days after hindlimb ischemia induction and day of administration), 7 14, 21, and 28 in mice injected with clustered myoblast cells, single myoblast cells, and saline (n = 10 each). *p < 0.05 versus saline group; †p < 0.05 versus single-cell group as analyzed by Tukey's *post hoc* test. Data are presented as the mean ± SEMs. (B) Representative LDPI images at days 0, 7, 14, and 28.

The number of centrally nucleated muscle fibers was significantly different among groups during the time course (Figure 5B). Centrally nucleated fibers are newly formed muscle fibers derived from satellite cells that are muscle progenitor cells.[21,22] The clustered-cell group had the highest number of centrally nucleated fibers at day 3. However, this gradually decreased and reached the lowest by day 28 during the time course and became quite rare at day 28. On the other hand, in the single-cell and saline groups, the number of centrally nucleated fibers was low at day 3, gradually increased, peaked at day 7, and remained high even at day 28.

The most significant number of embryonic myosin heavy chain (eMHC), a known marker of early stage muscle regeneration,[22–24] was detected in the clustered-cell group at day 3 (clustered cells, 53.8 ± 12.8/mm^2; single cells, 9.9 ± 3.8/mm^2; and saline, 3.2 ± 1.1/mm^2) (Figures 5C and 5D).

Expression of genes and protein related to muscle regeneration

The expression of genes related to muscle regeneration, including paired box 7 (*PAX7*), myogenic differentiation 1 (*MYOD1*), and myogenin (*MYOG*), is shown in Figure 5E. The expression of *PAX7*, a marker of satellite cells,[22] showed the most significant increase at day 7 in the clustered-cell group. *MYOD1,* a marker of differentiating satellite cells and myoblast cells,[25] was significantly upregulated at days 3 and 7 in the clustered-cell group compared with the saline group. Although the expression of *MYOG*, a marker of myotubes,[22] showed no significant difference, that in the clustered-cell group was relatively the lowest at day 28 (p = 0.057 versus single cells, p = 0.059, versus saline), indicating the completion of muscle regeneration. The protein expression level related to muscle regeneration was evaluated with western blotting using muscle harvested at day 7. Extracellular signal related-kinase 1/2 (ERK) and phosphorylated-ERK1/2 (p-ERK) were evaluated. Western blotting analysis showed that phosphorylation of ERK1/2 was significantly upregulated in the clustered cells group compared with the other groups (Figures 5F and 5G).

Together, these results showed that, in the clustered-cell group, the muscle regeneration process was significantly augmented early following administration and was almost completed within 28 days. In contrast, in the other two groups, muscle regeneration progressed more slowly and remained incomplete at day 28.

Direct differentiation of administered myoblast cells into skeletal muscle fibers

During the experiment using green fluorescent protein (GFP) positive myoblast cells, direct differentiation of administered myoblast cells into muscle fibers was detected in both single-cell and clustered-cell groups (Figure 4E), although this direct differentiation was infrequent with <1% of muscle fibers.

Inflammation and tissue-repairing process

Accelerated transition from pro-inflammatory to anti-inflammatory macrophages

To elucidate the mechanism underlying accelerated tissue repair, we evaluated the inflammatory status, especially macrophage polarization. Macrophages have multiple phenotypes that exert various effects, and their polarization into activated forms occurs during tissue repair.[26] Macrophage phenotypes are roughly classified into the proinflammatory M1 type and the anti-inflammatory M2 type. We determined the number of proinflammatory macrophages with CD11c and anti-inflammatory macrophages with CD206.[27]

The total number of macrophages increased within 4 days after induction of hindlimb ischemia and then decreased gradually, indicating that acute inflammation subsided when administration of cells was performed at day 0 (data not shown). The changes in the number and phenotype of macrophages following administration are shown in Figures 6A and 6B.

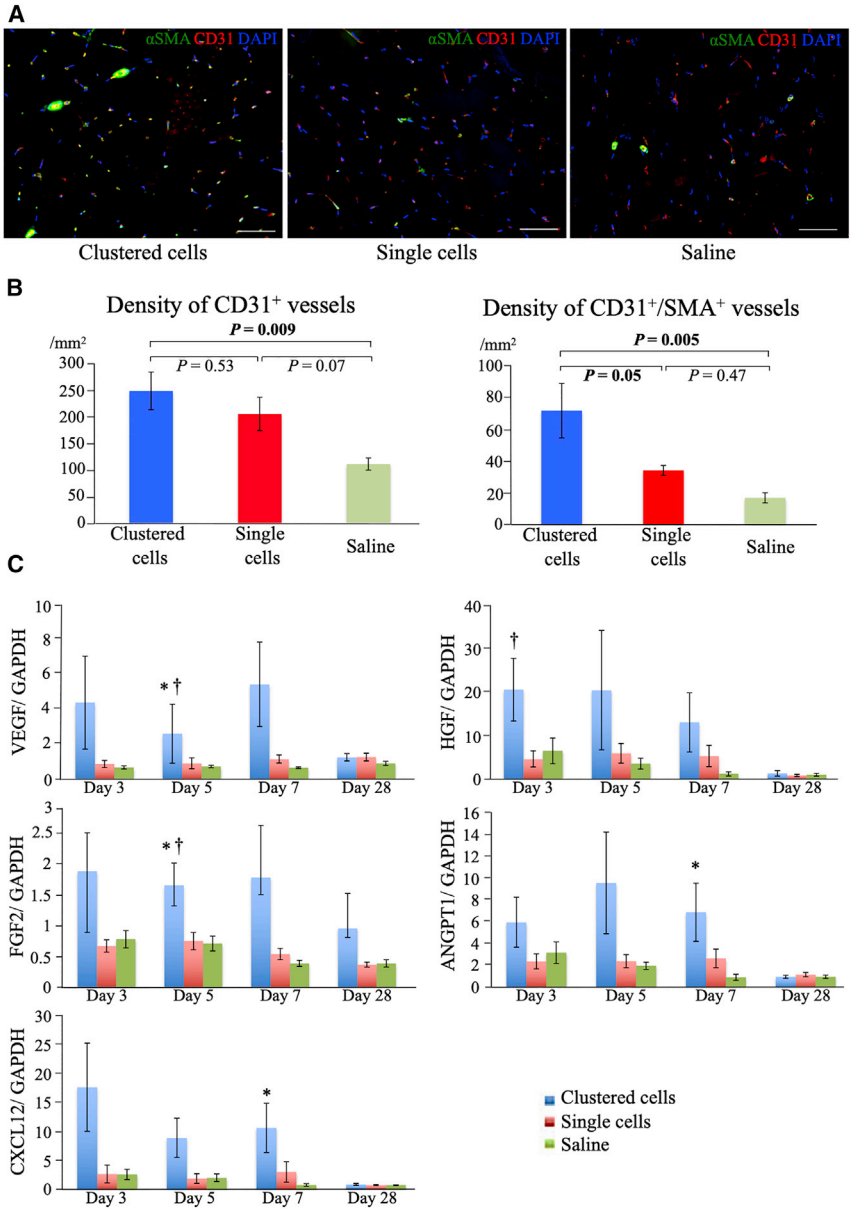

Figure 3. Angiogenesis induced by clustered cells

(A) Representative immunohistochemistry images of the microvasculature in ischemic muscles at 28 days after administration: anti-alpha SMA (green), CD31 (red), and nuclei (blue) at 28 days after administration. Scale bar: 50 μm. (B) Density of $CD31^+$ and $CD31^+/\alpha SMA^+$ vessels at 28 days after administration (n = 6 each). (C) Gene expression of angiogenesis-related factors in ischemic muscles measured using real-time PCR at days 3, 5, 7, and 28 (n = 6 each). *p < 0.05 versus saline group; †p < 0.05 versus single-cell group as analyzed by Tukey's *post hoc* test. Data are presented as the mean ± SEMs.

The total number of macrophages was the highest in the clustered-cell group within 7 days after administration but gradually decreased. At day 3, the number of $CD11c^+/CD206^+$ macrophages increased after clustered cells administration. At day 5, in the clustered-cell group, the number of anti-inflammatory $CD11c^-/CD206^+$ macrophages significantly increased (12.9 ± 2.3/mm^2 at day 3; 202.8 ± 25.1/mm^2 at day 5; $p < 0.0001$), whereas that of $CD11c^+/CD206^+$ macrophages decreased and was similar to that of the other two groups. At day 5, in the clustered-cell group, although the number of $CD11c^+/CD206^-$ macrophages did not significantly increase (105.2 ± 18.6/mm^2 at day 3 and 150.1 ± 40.5/mm^2 at day 5; $p = 0.5$), it was significantly larger than that of the other groups at day 5, suggesting that clustered cells administration induced macrophage polarization dominantly into the anti-inflammatory but partially into the proinflammatory phenotype. Then, the numbers of each macrophage phenotype decreased gradually.

At day 5, in the clustered-cell group, macrophages exhibited mixed population of these three different phenotypes, suggesting the simultaneous activation of various phenotypes during tissue regeneration, depending on the phase of regeneration (Figure 6C). On the contrary, in the saline group, the number of macrophages remained low but rather persistent within 28 days, indicating the prolonged inflammatory status. This was similarly observed in the single-cell group; however, the number of anti-inflammatory $CD11c^-/CD206^+$ macrophages remained relatively high at day 28, suggesting a therapeutic effect, albeit weak and slow acting.

Expression of genes related to inflammation and tissue repair

The gene expression of proinflammatory cytokines, including tumor necrosis factor-α (*TNF*), interleukin-1β (*IL1B*), and *IL6* (Figure 6F), showed no significant difference, although the clustered-cell group had the highest levels. We attribute this to the increased number of proinflammatory macrophages. *IL4*, which is a trigger for macrophage polarization into the anti-inflammatory phenotype,[26] was significantly increased at day 3 after clustered cells administration. The gene expression of anti-inflammatory cytokines, including *IL10* and transforming growth factor β1 (*TGFB1*), which are secreted by anti-inflammatory M2 macrophages, was the most significantly upregulated at days 5 and 7 in the clustered-cell group.

DISCUSSION

This study demonstrated that clustered cells formed using cell sheet technology improved the survival of administered cells and subsequently augmented angiogenesis and muscle regeneration.

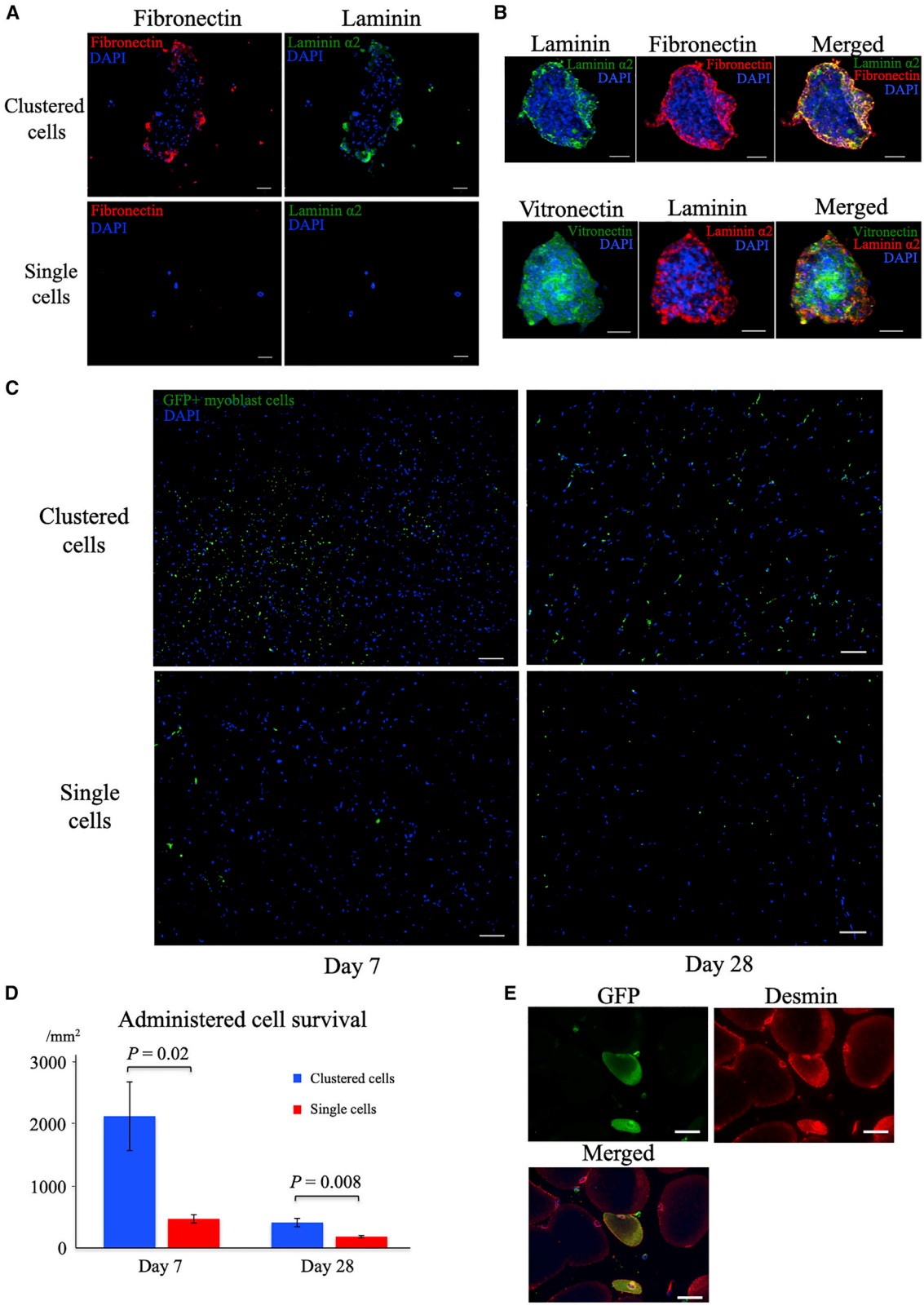

(legend on next page)

Furthermore, they regulated inflammation via macrophage polarization mainly into the anti-inflammatory phenotype.

We observed that the administration of clustered cells significantly improved blood perfusion and was associated with marked increases in gene expressions of angiogenesis-associated factors, including *VEGF*,[28,29] *FGF2*,[30] *HGF*,[31] *ANGPT1*,[29,32] and *CXCL12*.[25] Consistently, histological analysis showed superior angiogenesis effect as evaluated by $CD31^+/\alpha SMA^+$ arterioles, which are more mature vessels than $CD31^+$ capillaries. Moreover, remarkable muscle regeneration was detected following the administration of clustered myoblast cells. The number of centrally nucleated muscle fibers peaked at day 3, and muscle regeneration was almost completed within 28 days following the administration of clustered cells. In contrast, in the single-cell and saline groups, muscle regeneration was incomplete at day 28 after administration. A previous study has reported, after induction of hindlimb ischemia, full recovery as evidenced by blood perfusion, and muscular morphology required at least 56 days.[24] Thus, we speculate that the administration of clustered cells dramatically accelerated the muscle regeneration process. We also detected the significant activation of the ERK signaling pathway following the clustered cells administration. The ERK-mediated signaling pathway is reported to be important for both angiogenesis and muscle regeneration.[33,34]

The interaction between angiogenesis and muscle regeneration, two processes that occur simultaneously, is important for augmented regeneration.[22,35] In muscle regeneration, the activation, proliferation, and differentiation of satellite cells, which are the muscle progenitor cells, are prerequisites.[22] After muscle injuries, quiescent satellite cells are activated, proliferate, and then differentiate into myoblast cells, which fuse with damaged muscle fibers, thereby causing muscle regeneration.[22] In contrast, during angiogenesis, vascular endothelial cells secrete various growth factors, including VEGF, HGF, and FGF2, that promote the proliferation of satellite cells and myoblast cells in a paracrine fashion.[22,36–39] Additionally, satellite cells and myoblast cells also secrete VEGF and HGF to further enhance muscle regeneration in an autocrine fashion.[16,22] Through these paracrine and autocrine effects, muscle regeneration and angiogenesis were enhanced, following the administration of clustered cells.

Meanwhile, the continuous activation of satellite cells to differentiate into myoblast cells eventually leads to the loss of satellite cells and muscle regenerative capacity; therefore, the subsequent self-renewal of satellite cells, which is controlled by angiogenesis, is essential.[40,41] During angiogenesis, vascular endothelial cells extend and are located near satellite cells, and this proximity regulates the activation of satellite cells and then induces their self-renewal.[36,40] In this study, in the clustered-cell group, we detected increased *PAX7* at day 7 following *MYOD1* elevation, which peaked at day 3. Because *PAX7* is a marker of quiescent satellite cells,[22,25] we speculate that these events correspond to an augmented active muscle repair phase and the subsequent self-renewal phase of satellite cells, respectively, thus resulting in markedly augmented muscle regeneration.

The proper regulation of inflammation is important for healthy regeneration; in contrast, uncontrolled persistent inflammation leads to fibrosis and scarring.[42] Macrophages play pivotal roles in inflammatory response and have various phenotypes, such as proinflammatory M1, an anti-inflammatory M2, and intermediate phenotypes, including M1b ($CD11c^+/CD206^+$) macrophages.[27,43–46] In the clustered-cell group, we initially observed an increase in the number of intermediate $CD11c^+/CD206^+$ macrophages, followed by partial polarization into M1 and dominant polarization into M2 macrophages at day 5. Among the various triggers of macrophage polarization, *IL4*, a classic trigger for polarization into the anti-inflammatory phenotype,[26] was significantly increased at day 3 after the administration of clustered cells. Additionally, the phagocytosis of residual damaged cells by increased macrophages,[22,47] increased number of endothelial cells during angiogenesis,[48] and administration of the ECM scaffold, which is included in clustered cells,[49–51] would have induced polarization into the anti-inflammatory phenotype. Administration of ECM can affect macrophage polarization through its structural components, scaffold resident growth factors, and interactive signaling among the surface receptors of macrophages and the ECM.[52]

Although anti-inflammatory macrophages play a pivotal role in tissue regeneration, their partial and temporal polarization into proinflammatory macrophages, which we have detected in this study, would be also important for tissue regeneration. Although the persistent existence of proinflammatory macrophages negatively affects angiogenesis, their short-term presence positively affects tissue repair in various ways: activating endothelial tip cells to promote angiogenesis[26]; phagocytosing injured muscle debris, which in turn induces a phenotype switch into the anti-inflammatory phenotype[22,47]; and enhancing the proliferation of satellite cells to promote muscle regeneration.[47,53] Anti-inflammatory macrophages, which we detected as dominant, secrete VEGF and TGF-β that promote the formation of mature $CD31^+/\alpha\text{-}SMA^+$ vessels.[54] Anti-inflammatory macrophages also accelerate muscle regeneration by secreting TGF-β to activate fibronectin, laminin, and proteoglycans, which bind to collagen types I and III at the injured sites, thus forming a temporary ECM.[20,42,55,56] The temporary ECM and basement membrane of injured muscles provide a suitable environment for myoblast differentiation and act

Figure 4. Extracellular matrix included in clustered cells and cell tracking after administration

(A) Representative immunohistochemistry images of the extracellular matrix included in clustered myoblast cells and single myoblast cells (acetic acid/ethanol fixation of scattered cells): fibronectin (red), laminin (green), and nuclei (blue). Scale bars: 50 μm. (B) Magnified view of cell clusters stained with antibodies against laminin, fibronectin, and vitronectin. Upper row: laminin (green), fibronectin (red), and nuclei (blue); bottom row: vitronectin (green), laminin (red), and nuclei (blue). Scale bars: 50 μm. (C) Survival of clustered and single myoblast cells derived from enhanced GFP-transgenic mice at days 7 and 28. Scale bars: 50 μm. (D) Density of surviving myoblast cells at days 7 and 28 (n = 4 each). Data are presented as the mean ± SEMs. (E) Differentiation of administered GFP^+ myoblast cells into muscle fibers at day 7: GFP (green) and desmin (red). Scale bar: 50 μm.

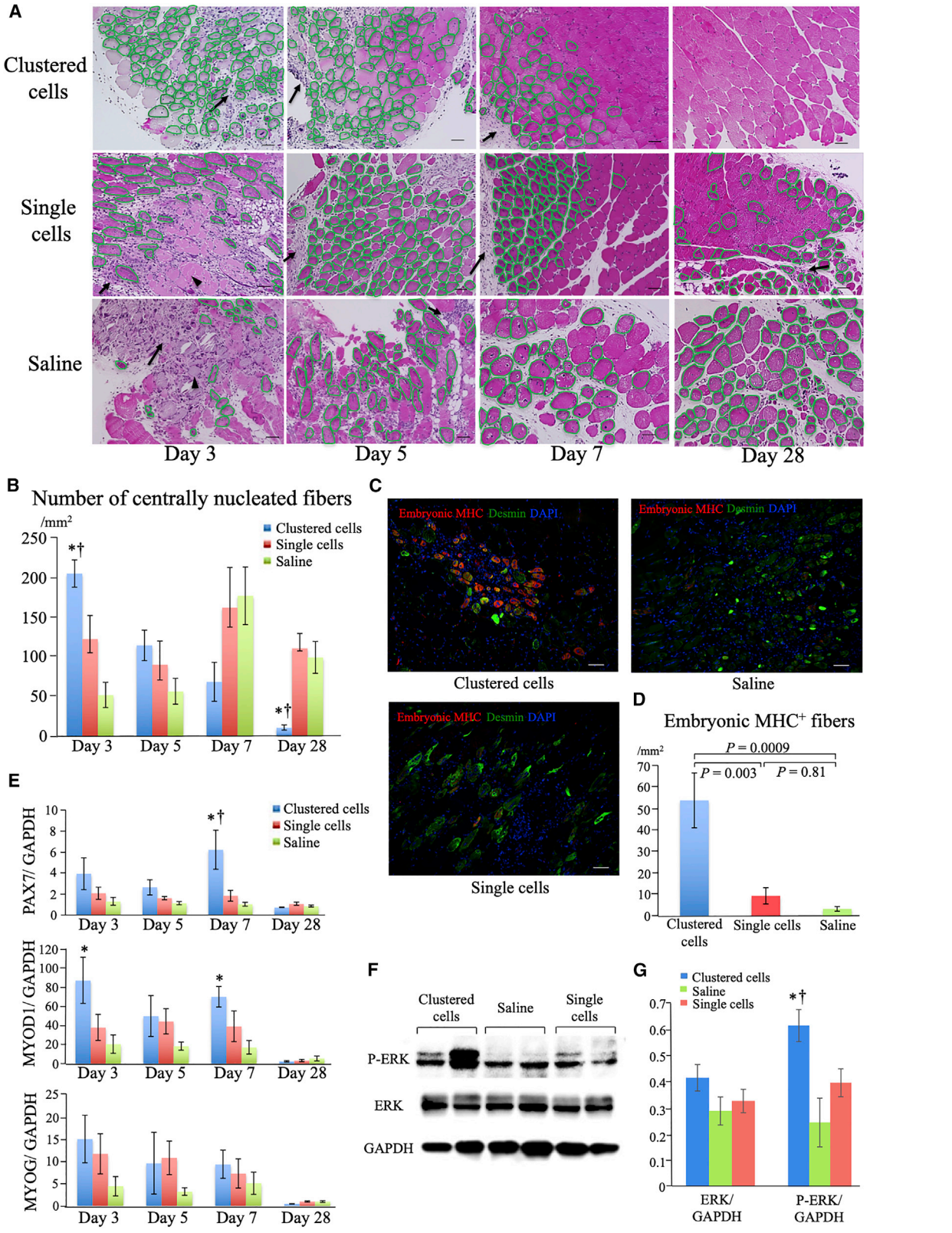

(legend on next page)

as a scaffold for muscle fiber regeneration.[20,42] By balancing the temporary ECM formation and degradation, ECM remodeling occurs, which is essential for angiogenesis and muscle regeneration; this balance is regulated by both proinflammatory and anti-inflammatory macrophages.[20]

Furthermore, the administration of clustered cells improved the survival of administered myoblast cells and subsequently augmented tissue regeneration. *In vitro* study comparing the clustered cells and the single cells using ELISA showed that production ability of angiogenesis-related cytokines, including VEGF, HGF, CXCL12, and FGF2, was not significantly different between the groups (data not shown). This result would support the theory that improved cell survival is the major contributor to the enhanced tissue repair. Enhanced cells survival is attributed to the ECM that surrounds the myoblast cells. In addition to the anti-apoptotic effect exerted by laminin and vitronectin by maintaining intracellular signaling among administered cells,[17,57] the administered ECM, including laminin, vitronectin, and fibronectin, functions as an adhesive agent to the injured sites.[17,58,59] Fibronectin formed in the clustered cells can also act as a scaffold for endothelial cells to aggregate and form new vessels,[18,60,61] which may in turn promote blood perfusion to administered cells and may contribute to improved cell survival.

The proposed mechanisms of augmented tissue regeneration following the administration of clustered myoblast cells is illustrated in Figure 7. Overall, clustered myoblast cells created using cell sheet technology improved the survival of administered cells, leading to the augmented secretion of cytokines that promote both angiogenesis and muscle regeneration. Additionally, clustered cells administration modulated the inflammatory status by inducing macrophage polarization, thus establishing a suitable microenvironment for tissue regeneration.

In summary, we demonstrated that clustered cells synthesized using cell sheet technology improved the survival of administered myoblast cells in a mouse model of limb ischemia. The number of macrophages increased, and their polarization into a dominant anti-inflammatory phenotype was detected, thus promoting angiogenesis and muscle regeneration. We are now investigating the applicability of the clustered cell technology for another cell type, and the result is positive so far. The clustered cell technology will augment regenerative effect of various cell therapy. Our findings suggest clinical potential of rescuing severely damaged limbs in PAD using clustered cells.

MATERIALS AND METHODS

Animals and ethical considerations

C57BL/6J male mice (4- or 8-week-old) and enhanced GFP (eGFP)-transgenic male mice (C57BL/6J background) were used. Wild-type C57BL/6J mice were purchased from CLEA Japan (Osaka, Japan) and eGFP-transgenic mice were from Japan SLC (Shizuoka, Japan). All animal experiments were performed according to the *Guide for the Care and Use of Laboratory Animals* (National Institutes of Health publication No. 85-23, revised 1996). Experimental protocols were approved by the Animal Experiments Committee of Osaka University.

Isolation and culture of myoblast cells and generation of clustered cells

Myoblast cells were isolated from the skeletal muscles of the hind limbs of 4-week-old wild-type C57BL/6J mice or eGFP-transgenic C57BL/6J mice and cultured as previously reported.[62] At 70% confluence, cells were dissociated from the culture dishes using trypsin-ethylenediaminetetraacetic acid and re-incubated (1.0×10^6 per dish) on 12.8 mm temperature-responsive culture dishes (UpCell; CellSeed, Tokyo, Japan) at 37°C. After 24 h, the dishes were incubated at 20°C for 30 min, during which the myoblast cell sheets detached spontaneously to generate free-floating monolayer cell sheets. To produce an injectable form, each cell sheet was fragmented and mixed with 0.3 mL saline by five times repetitive aspiration and expiration using 1 mL syringe through a 23-gauge needle, forming clustered myoblast cells (Figures 1A–1E).

Flow cytometry

Cultured cells were enzymatically dissociated using TrypLE Select (Thermo Fisher Scientific, MA, USA), washed, and labeled with fluorescence-conjugated primary antibodies for CD56 for 30 min at 4°C. The samples were then assayed by flow cytometry (FACSCanto II; BD Biosciences, CA), and the results were analyzed using BD FACSDiva Software (BD Biosciences). As a result, more than 90% of the cultured cells were $CD56^+$.

ELISA

The difference in cytokine production between clustered cells and single cells was analyzed with ELISA. Clustered myoblast cells and single myoblast cells were disseminated on 12-well plates (Iwaki, Shizuoka, Japan) (1.0×10^6 per well) and incubated at 37°C for 48 h. The culture supernatants were collected and analyzed. VEGF, HGF, SDF-1, and FGF-2 concentrations were evaluated using ELISA kit (R&D Systems, MN, USA) according to the manufacturer's protocol.

Figure 5. Muscle regeneration induced by clustered cells administration

(A) Representative images of H&E-stained ischemic muscles following the administration of clustered cells, single cell, or saline groups at days 3, 5, 7, and 28 after administration. Arrows indicate cell infiltration into the temporary ECM, whereas arrowheads indicate lysis of damaged muscle fibers. Muscle fibers encircled with green lines indicate centrally nucleated fibers. Scale bars: 50 μm. (B) Numbers of centrally nucleated fibers at days 3, 5, 7, and 28 (n = 6 each). *p < 0.05 versus saline group; †p < 0.05 versus single-cell group as analyzed by Tukey's *post hoc* test. (C) Representative immunohistochemistry images of ischemic muscles at day 3: embryonic myosin heavy chain (MHC) (pseudo-colored red), desmin (green), and nuclei (blue). Scale bars: 50 μm. (D) Numbers of embryonic MHC^+ muscle fibers at day 3 (n = 6 each). (E) Expression of genes related to skeletal muscle regeneration related factors in ischemic muscles at days 3, 5, 7, and 28 measured using real-time PCR (n = 6 each). *p < 0.05 versus saline group; †p < 0.05 versus single-cell group as analyzed by Tukey's *post hoc* test. (F) Protein expression levels of ERK and phosphorylated ERK (P-ERK) measured by western blot using ischemic muscles at day 7 after administration. (G) Quantification of protein expression levels at day 7 after administration (n = 4 each). *p < 0.05 versus saline group; †p < 0.05 versus single-cell group as analyzed by Tukey's *post hoc* test. Data are presented as the mean ± SEMs.

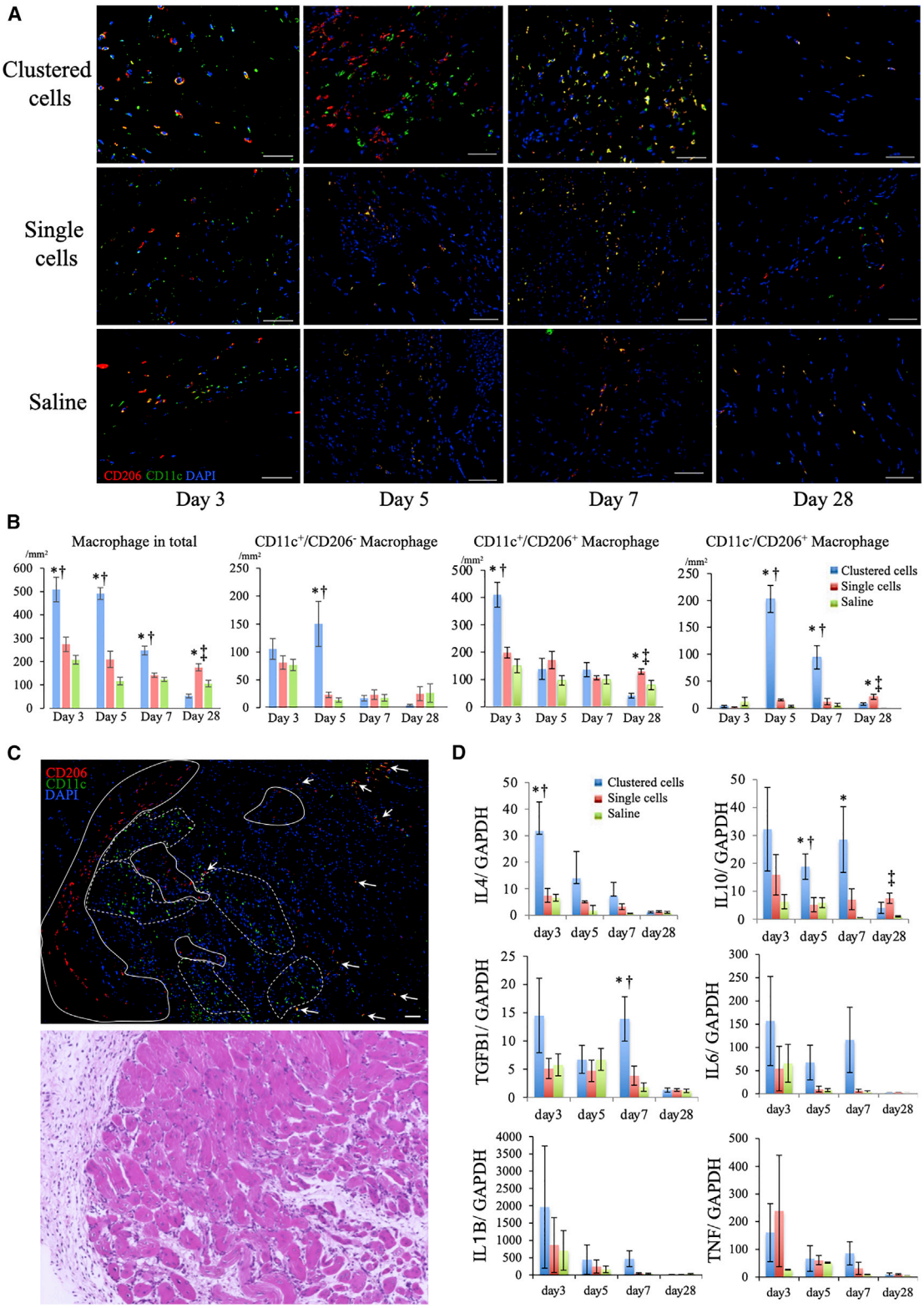

(legend on next page)

Induction of hindlimb ischemia and therapeutic intervention

C57B/6J mice (8-week-old) were anesthetized by an intraperitoneal administration of combination anesthetic (medetomidine/midazolam/butorphanol: 0.3/4/5) at a dose of 5 mL/kg. Hindlimb ischemia was induced in the left hindlimb by exposing and ligating the femoral artery and vein at the level of the inguinal ligament and the saphenous artery and vein at the level just proximal to the ankle, and then by resecting all the vessels among ligations.

One week after induction of ischemia, blood perfusion was measured using LDPI, and mice with LDPI relative value of $\leq$25% of the non-ischemic limb were subjected to treatment interventions. Using the strict criteria, we selected only the mice with severely impaired blood perfusion with limited automatic angiogenesis ability, to evaluate the regenerative efficacy genuinely attributable to the cell therapy. Then, mice were randomly allotted into three groups: administration of clustered myoblast cells, single myoblast cells, and saline. The single-cell group was injected with the same number of myoblast cells (1.0×10^6 cells) as the clustered-cell group. Administered cells were mixed with 0.3 mL saline. Cell injection was performed into the ischemic thigh adductors 1 week after the induction of limb ischemia (Figure 1F).

Evaluation of blood perfusion using LDPI

Blood perfusion was evaluated using the Laser Doppler Imager 2.0 system (Moor Instruments, Devon, UK) at pre-ligation, at post-ligation, just before administration (7 days after ligation), and at 1, 2, 3, and 4 weeks after administration. Mice were first anesthetized through inhalation of 2% isoflurane/oxygen. The relative perfusion value was calculated by dividing the perfusion value of the ischemic limb by that of the contralateral non-ischemic limb.

Histological and immunofluorescence analysis

The harvested adductor muscles were formalin-fixed, made into paraffin embedded, sectioned into 5 μm using a microtome, and stained with H&E. To evaluate the morphometrics of the ischemic muscles, images were visualized using an optical microscopy (KEYENCE, Osaka, Japan).

For the immunohistochemical analysis, muscles were fixed with 4% paraformaldehyde and embedded in optimal cutting temperature compound for frozen sectioning and cut into 5 μm. The sections were labeled with polyclonal antibodies against CD31 (Abcam, Cambridge, UK) and visualized using an LSABTM kit (DAKO, Glostrup, Denmark), an automated immuno-staining system based on the lepto-streptavidin-biotin-peroxidase method. Sections were additionally labeled using antibodies, including SMA (DAKO), desmin (DAKO), and embryonic MHC (Cell Signaling Technology, MA, USA), CD206 (Abcam), CD11c (Abcam), and anti-GFP (Abcam), and the corresponding secondary antibodies (Alexa Fluor 488 or Alexa Fluor 555, Molecular Probes, OR, USA). Then, they were counterstained by Hoechst 33,342 (Dojindo, Kumamoto, Japan) and visualized using laser confocal microscopy (Olympus, Tokyo, Japan).

Muscle fibers were counted from five randomly selected fields per sample at 20× magnification. The percentage of centrally nucleated fibers was calculated by dividing the number of centrally nucleated fibers by the total number of fibers. The numbers of $CD31^+$ capillaries and $CD31^+/\alpha SMA^+$ arterioles were also counted from five randomly selected 20× images per sample.

For the macrophages, polyclonal antibodies against CD11c and CD206 were used. To evaluate the number of macrophages located in the temporary ECM among muscle fibers, which is formed during tissue repair,[20] we determined the number of $CD11c^+/CD206^-$, $CD11c^+/CD206^+$, and $CD11c^-/CD206^+$ macrophages from five randomly selected fields per sample at 40× magnification. The total number of macrophages was calculated by adding all these three phenotypes.

Evaluation of cell survival and differentiation

The observation of cell survival and lineage tracing of administered cells were performed by injecting 4-week-old eGFP-transgenic mice derived myoblast cells into ischemic adductor muscles of hindlimb ischemia models. After 1 and 4 weeks after administration, mice were euthanized; adductor muscles were harvested and the existence of GFP^+ myoblast cells was counted using five randomly selected images per sample at 40× magnification.

RNA isolation and quantitative real-time PCR

Total RNA was extracted from the adductor muscles using an RNeasy Kit according to the manufacturer's protocol (Qiagen, Hilden, Germany). Then, cDNA was synthesized using an Omniscript Reverse Transcription Kit (Qiagen). Real-time PCR was performed with the TaqMan Gene Expression Assay Master Mix (Applied Biosystems, CA, USA) on the 7500 Fast Real-Time PCR System (Applied Biosystems).

The following genes were analyzed using the TaqMan Gene Expression Assay (Applied Biosystems): *VEGF* (Mm01281449_m1), *HGF* (Mm01135184_m1), *FGF2* (Mm01281449_m1), *CXCL12* (Mm004545553_m1), *ANGPT1* (Mm00833184_s1), *PAX7* (Mm 01354484_m1), *MYOD1* (Mm00521984_m1), *MYOG* (Mm00446194_ m1), *TNF* (Mm00443258_m1), *TGFB1*B(Mm01178820_m1), *IL1Bβ*

Figure 6. Modulation of inflammation induced by clustered cells

(A) Representative immunohistochemistry images of macrophages in ischemic muscles at days 3, 5, 7, and 28: anti-CD206 (red), anti-CD11c (green), and nuclei (blue). Scale bars: 50 μm. (B) Density of macrophages at days 3, 5, 7, and 28. *p < 0.05 versus saline group;†p < 0.05 versus single-cell group; ‡p < 0.05 versus clustered-cell group as analyzed by Tukey's *post hoc* test. (C) Top: representative immunohistochemistry images of macrophages at day 5 after administration of clustered cells: anti-CD206 (red), anti-CD11c (green), and nuclei (blue). Bottom: corresponding images with H&E staining. The clusters of anti-inflammatory $CD11c^-/CD206^+$ macrophages are encircled in solid lines; proinflammatory $CD11c^+/CD206^-$macrophages, broken lines; and intermediate $CD11c^+/CD206^+$ macrophages, indicated by arrows. Scale bar: 50 μm. (D) Gene expression of inflammation-associated factors in ischemic muscles at days 3, 5, 7, and 28 measured using real-time PCR (N = 6 each). *p < 0.05 versus saline group; †p < 0.05 versus single-cell group as analyzed by Tukey's *post hoc* test. Data are shown as the mean ± SEMs.

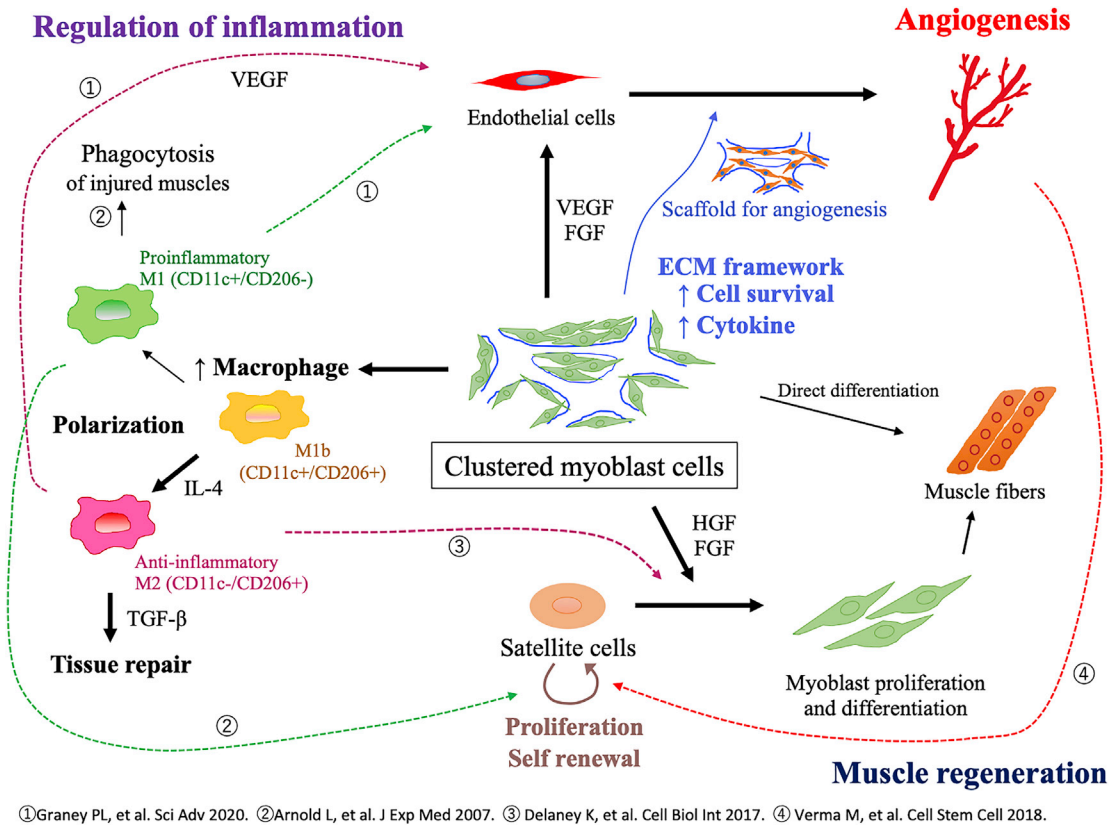

Figure 7. Mechanism of tissue regeneration induced by clustered cells
Proposed mechanism of angiogenesis and muscle regeneration following the administration of clustered myoblast cells.

(Mm00434228_m1), *IL6* (Mm00446190_m1), and *IL10* (Mm 00439614_m1). Glyceraldehyde-3-phosphate dehydrogenase (GAPDH) (Mm99999915_g1) was co-amplified as an internal control for RNA integrity.

Western blotting

For western blotting, 100 μg of protein acquired from the collected muscles was electrophoresed with PROTEAN precast gels (Bio-Rad Laboratories, CA, USA) and transferred to a polyvinylidene fluoride blotting membrane (GE Healthcare Life Sciences, MA, USA). The membrane was incubated with the primary antibody overnight, followed by incubation with the secondary antibody. Signals were detected and visualized using Amersham enhanced chemiluminescence (ECL) Prime western blotting detection reagent (GE Healthcare). Luminescence was detected using the ChemiDoc MP Imaging System (Bio-Rad). Quantification of bands intensity was performed with Image Lab software version 5.0 (Bio-Rad). Ischemic muscles harvested at day 7 were used for analysis. The following antibodies were analyzed: anti-p-ERK (#4370), anti-ERK1/2 (1:1000; Cell Signaling Technology), and anti-GAPDH (1:10000; Cell Signaling Technology). Amersham ECL anti-rabbit immunoglobulin G (GE Healthcare) was used as a secondary antibody at a dilution of 1:10000.

Statistical analysis

Multiple comparisons of LDPI values, real-time PCR data, and muscles and vessel counts were performed using the analysis of variance followed by a Tukey's *post hoc* test. Data are presented as the mean ± SEM, unless otherwise noted. $p < 0.05$ indicates statistical significance. JMP (version 13.1, SAS Institute, NC, USA) was used for the statistical analyses.

ACKNOWLEDGMENTS

This work is supported by the Japan Society for the Promotion of Science (JSPS) KAKENHI Grant Number JP20K17150.

AUTHOR CONTRIBUTIONS

K.M. and A.H. conducted the experiments; K.M. wrote the pater; K.M., S.M., and Y.S. designed the experiments.

DECLARATION OF INTERESTS

None.

REFERENCES

1. Fowkes, F.G.R., Rudan, D., Rudan, I., Aboyans, V., Denenberg, J.O., McDermott, M.M., Norman, P.E., Sampson, U.K.A., Williams, L.J., Mensah, G.A., et al. (2013). Comparison of global estimates of prevalence and risk factors for peripheral artery disease in 2000 and 2010: a systematic review and analysis. Lancet *382*, 1329–1340.

2. Conte, M.S., Bradbury, A.W., Kolh, P., White, J.v., Dick, F., Fitridge, R., Mills, J.L., Ricco, J.B., Suresh, K.R., Murad, M.H., et al. (2019). Global vascular guidelines on the management of chronic limb-threatening ischemia. J. Vasc. Surg. *69*, 3S–125S.e40.

3. Norgren, L., Hiatt, W.R.R., Dormandy, J.A., Nehler, M.R.R., Harris, K.A., and Fowkes, F.G.R.; TASC II Working Group (2007). Inter-society consensus for the management of peripheral arterial disease (TASC II). J. Vasc. Surg. *45* (*Suppl S*), S5–S67.

4. Lederman, R.J., Mendelsohn, F.O., Anderson, R.D., Saucedo, J.F., Tenaglia, A.N., Hermiller, J.B., Hillegass, W.B., Rocha-Singh, K., Moon, T.E., Whitehouse, M.J., et al. (2002). Therapeutic angiogenesis with recombinant fibroblast growth factor-2 for intermittent claudication (the TRAFFIC study): a randomised trial. Lancet *359*, 2053–2058.

5. Matoba, S., Tatsumi, T., Murohara, T., Imaizumi, T., Katsuda, Y., Ito, M., Saito, Y., Uemura, S., Suzuki, H., Fukumoto, S., et al. (2008). Long-term clinical outcome after intramuscular implantation of bone marrow mononuclear cells (Therapeutic Angiogenesis by Cell Transplantation [TACT] trial) in patients with chronic limb ischemia. Am. Heart J. *156*, 1010–1018.

6. Huang, P., LI, S., Han, M., Xiao, Z., and Yang Renchi, C.H.Z. (2005). Autologous transplantation of granulocyte colony – stimulating factor – cells improves critical limb ischemia in. Emerg. Treat. Technol. *28*, 2155–2160.

7. Teraa, M., Sprengers, R.W., Schutgens, R.E.G., Slaper-Cortenbach, I.C.M., van der Graaf, Y., Algra, A., van der Tweel, I., Doevendans, P.A., Mali, W.P.T.M., Moll, F.L., et al. (2015). Effect of repetitive intra-arterial infusion of bone marrow mononuclear cells in patients with no-option limb ischemia: the randomized, double-blind, placebo-controlled Rejuvenating Endothelial Progenitor Cells via Transcutaneous Intra-arterial Supplement. Circulation *131*, 851–860.

8. Losordo, D.W., Kibbe, M.R., Mendelsohn, F., Marston, W., Driver, V.R., Sharafuddin, M., Teodorescu, V., Wiechmann, B.N., Thompson, C., Kraiss, L., et al. (2012). A randomized, controlled pilot study of autologous CD34+ cell therapy for critical limb ischemia. Circ. Cardiovasc. Interv. *5*, 821–830.

9. Qadura, M., Terenzi, D.C., Verma, S., Al-Omran, M., and Hess, D.A. (2018). Concise review: cell therapy for critical limb ischemia: an integrated review of preclinical and clinical studies. Stem Cells *36*, 161–171.

10. Aboyans, V., Ricco, J.-B., Bartelink, M.-L.E.L., Björck, M., Brodmann, M., Cohnert, T., Collet, J.-P., Czerny, M., de Carlo, M., Debus, S., et al. (2018). Editor's choice – 2017 ESC guidelines on the diagnosis and treatment of peripheral arterial diseases, in collaboration with the European society for vascular surgery (ESVS). Eur. J. Vasc. Endovasc. Surg. *55*, 305–368.

11. Ungerleider, J.L., Johnson, T.D., Hernandez, M.J., Elhag, D.I., Braden, R.L., Dzieciatkowska, M., Osborn, K.G., Hansen, K.C., Mahmud, E., and Christman, K.L. (2016). Extracellular matrix hydrogel promotes tissue remodeling, arteriogenesis, and perfusion in a rat hindlimb ischemia model. JACC Basic Transl. Sci. *1*, 32–44.

12. Simons, J.P., Schanzer, A., Flahive, J.M., Osborne, N.H., Mills, J.L., Bradbury, A.W., and Conte, M.S. (2019). Survival prediction in patients with chronic limb-threatening ischemia who undergo infrainguinal revascularization. J. Vasc. Surg. *69* (6S), 137S–151S.

13. Miyake, K., Kikuchi, S., Tatsukawa, T., Uchida, D., Koya, A., Sawa, Y., and Azuma, N. (2020). Predictive model for postoperative ambulatory function after lower extremity bypass in chronic limb-threatening ischemia. Ann. Vasc. Surg. *71*, 321–330.

14. Miyagawa, S., Saito, A., Sakaguchi, T., Yoshikawa, Y., Yamauchi, T., Imanishi, Y., Kawaguchi, N., Teramoto, N., Matsuura, N., Iida, H., et al. (2010). Impaired myocardium regeneration with skeletal cell sheets-A preclinical trial for tissue-engineered regeneration therapy. Transplantation *90*, 364–372.

15. Kushida, A., Yamato, M., Konno, C., Kikuchi, A., Sakurai, Y., and Okano, T. (1999). Decrease in culture temperature releases monolayer endothelial cell sheets together with deposited fibronectin matrix from temperature-responsive culture surfaces. J. Biomed. Mater. Res. *45*, 355–362.

16. Miyagawa, S., Sawa, Y., Sakakida, S., Taketani, S., Kondoh, H., Memon, I.A., Imanishi, Y., Shimizu, T., Okano, T., and Matsuda, H. (2005). Tissue cardiomyoplasty using bioengineered contractile cardiomyocyte sheets to repair damaged myocardium: their integration with recipient myocardium. Transplantation *80*, 1586–1595.

17. Uchinaka, A., Tasaka, K., Mizuno, Y., Maeno, Y., Ban, T., Mori, S., Hamada, Y., Miyagawa, S., Saito, A., Sawa, Y., et al. (2017). Laminin α2-secreting fibroblasts enhance the therapeutic effect of skeletal myoblast sheets. Eur. J. Cardiothorac. Surg. *51*, 457–464.

18. Uemura, A., Kusuhara, S., Wiegand, S.J., Yu, R.T., and Nishikawa, S.I. (2006). Tlx acts as a proangiogenic switch by regulating extracellular assembly of fibronectin matrices in retinal astrocytes. J. Clin. Invest. *116*, 369–377.

19. Carrabba, M., de Maria, C., Oikawa, A., Reni, C., Rodriguez-Arabaolaza, I., Spencer, H., Slater, S., Avolio, E., Dang, Z., Spinetti, G., et al. (2016). Design, fabrication and perivascular implantation of bioactive scaffolds engineered with human adventitial progenitor cells for stimulation of arteriogenesis in peripheral ischemia. Biofabrication *8*, 015020.

20. Mann, C.J., Perdiguero, E., Kharraz, Y., Aguilar, S., Pessina, P., Serrano, A.L., and Muñoz-Cánoves, P. (2011). Aberrant repair and fibrosis development in skeletal muscle. Skeletal Muscle *1*, 1–20.

21. Collins, C.A., Olsen, I., Zammit, P.S., Heslop, L., Petrie, A., Partridge, T.A., and Morgan, J.E. (2005). Stem cell function, self-renewal, and behavioral heterogeneity of cells from the adult muscle satellite cell niche. Cell *122*, 289–301.

22. Yin, H., Price, F., and Rudnicki, M.A. (2013). Satellite cells and the muscle stem cell niche. Physiol. Rev. *93*, 23–67.

23. Karsch-Mizrachi, I., Travis, M., Blau, H., and Leinwand, L.A. (1989). Expression and DNA sequence analysis of a human embryonic skeletal muscle mvosin heavy chain gene. Nucleic Acids Res. *17*, 6167–6179.

24. Mohiuddin, M., Lee, N.H., Moon, J.Y., Han, W.M., Anderson, S.E., Choi, J.J., Shin, E., Nakhai, S.A., Tran, T., Aliya, B., et al. (2019). Critical limb ischemia induces remodeling of skeletal muscle motor unit, myonuclear-, and mitochondrial-domains. Sci. Rep. *9*, 9551.

25. Kozakowska, M., Kotlinowski, J., Grochot-Przeczek, A., Ciesla, M., Pilecki, B., Derlacz, R., Dulak, J., and Jozkowicz, A. (2015). Myoblast-conditioned media improve regeneration and revascularization of ischemic muscles in diabetic mice. Stem Cell Res. Ther. *6*, 1–16.

26. Graney, P.L., Ben-Shaul, S., Landau, S., Bajpai, A., Singh, B., Eager, J., Cohen, A., Levenberg, S., and Spiller, K.L. (2020). Macrophages of diverse phenotypes drive vascularization of engineered tissues. Sci. Adv. *6*, eaay6391.

27. Gambaro, S.E., Zubiría, M.G., Portales, A.E., Rey, M.A., Rumbo, M., and Giovambattista, A. (2018). M1 macrophage subtypes activation and adipocyte dysfunction worsen during prolonged consumption of a fructose-rich diet. J. Nutr. Biochem. *61*, 173–182.

28. Gerber, H.P., Malik, A.K., Solar, G.P., Sherman, D., Liang, X.H., Meng, G., Hong, K., Marsters, J.C., and Ferrara, N. (2002). VEGF regulates haematopoietic stem cell survival by an internal autocrine loop mechanism. Nature *417*, 954–958.

29. Carmeliet, P. (2003). Angiogenesis in health and disease. Nat. Med. *9*, 653–660.

30. Arvidsson, A., Collin, T., Kirk, D., Kokaia, Z., and O, L. (2003). Neuronal replacement from endogenous precursors in the adult. Nat. Med. *9*, 548–553.

31. Van Belle, E., Witzenbichler, B., Chen, D., Silver, M., Chang, L., Schwall, R., and Isner, J.M. (1998). Potentiated angiogenic effect of scatter factor/hepatocyte growth factor via induction of vascular endothelial growth factor: the case for paracrine amplification of angiogenesis. Circulation *97*, 381–390.

32. Jain, R.K., and Munn, L.L. (2000). Leaky vessels? Call Ang1! Nat. Med. *6*, 131–132.

33. Song, M., and Finley, S.D. (2020). ERK and Akt exhibit distinct signaling responses following stimulation by pro-angiogenic factors. Cell Commun. Signal. *18*, 1–19.

34. Jiang, W., Zhu, J., Zhuang, X., Zhang, X., Luo, T., Esser, K.A., and Ren, H. (2015). Lipin1 regulates skeletal muscle differentiation through extracellular signal-regulated kinase (ERK) activation and cyclin D complex-regulated cell cycle withdrawal. J. Biol. Chem. *290*, 23646–23655.

35. Luque, E., Peña, J., Martin, P., Jimena, I., and Vaamonde, R. (1995). Capillary supply during development of individual regenerating muscle fibers. Anat. Histol. Embryol. *24*, 87–89.

36. Christov, C., Chrétien, F., Abou-Khalil, R., Bassez, G., Vallet, G., Authier, F.-J., Bassaglia, Y., Shinin, V., Tajbakhsh, S., Chazaud, B., et al. (2007). Muscle satellite cells and endothelial cells: close neighbors and privileged partners. Mol. Biol. Cell *18*, 1397–1409.

37. Arsic, N., Zacchigna, S., Zentilin, L., Ramirez-Correa, G., Pattarini, L., Salvi, A., Sinagra, G., and Giacca, M. (2004). Vascular endothelial growth factor stimulates skeletal muscle regeneration in Vivo. Mol. Ther. *10*, 844–854.

38. Cornelison, D.D.W., Filla, M.S., Stanley, H.M., Rapraeger, A.C., and Olwin, B.B. (2001). Syndecan-3 and syndecan-4 specifically mark skeletal muscle satellite cells and are implicated in satellite cell maintenance and muscle regeneration. Dev. Biol. *239*, 79–94.

39. Allen, R.E., Sheehan, S.M., Taylor, R.G., Kendall, T.L., and Rice, G.M. (1995). Hepatocyte growth factor activates quiescent skeletal muscle satellite cells in vitro. J. Cell Physiol. *165*, 307–312.

40. Verma, M., Asakura, Y., Murakonda, B.S.R., Pengo, T., Latroche, C., Chazaud, B., McLoon, L.K., and Asakura, A. (2018). Muscle satellite cell cross-talk with a vascular niche maintains quiescence via VEGF and notch signaling. Cell Stem Cell *23*, 530–543.e9.

41. Chakkalakal, J.V., Jones, K.M., Basson, M.A., and Brack, A.S. (2012). The aged niche disrupts muscle stem cell quiescence. Nature *490*, 355–360.

42. Mahdy, M.A.A. (2019). Skeletal muscle fibrosis: an overview. Cell Tissue Res. *375*, 575–588.

43. Morris, D.L., Singer, K., and Lumeng, C.N. (2011). Adipose tissue macrophages: phenotypic plasticity and diversity in lean and obese states. Curr. Opin. Clin. Nutr. Metab. Care *14*, 341–346.

44. Wentworth, J.M., Naselli, G., Brown, W.A., Doyle, L., Phipson, B., Smyth, G.K., Wabitsch, M., O'Brien, P.E., and Harrison, L.C. (2010). Pro-inflammatory CD11c+CD206+ adipose tissue macrophages are associated with insulin resistance in human obesity. Diabetes *59*, 1648–1656.

45. Shaul, M.E., Bennett, G., Strissel, K.J., Greenberg, A.S., and Obin, M.S. (2010). Dynamic, M2-like remodeling phenotypes of CD11c+ adipose tissue macrophages during high-fat diet - induced obesity in mice. Diabetes *59*, 1171–1181.

46. Shapouri-Moghaddam, A., Mohammadian, S., Vazini, H., Taghadosi, M., Esmaeili, S.A., Mardani, F., Seifi, B., Mohammadi, A., Afshari, J.T., and Sahebkar, A. (2018). Macrophage plasticity, polarization, and function in health and disease. J. Cell Physiol. *233*, 6425–6440.

47. Arnold, L., Henry, A., Poron, F., Baba-Amer, Y., Van Rooijen, N., Plonquet, A., Gherardi, R.K., and Chazaud, B. (2007). Inflammatory monocytes recruited after skeletal muscle injury switch into antiinflammatory macrophages to support myogenesis. J. Exp. Med. *204*, 1057–1069.

48. Zhang, J., Muri, J., Fitzgerald, G., Gorski, T., Gianni-Barrera, R., Masschelein, E., D'Hulst, G., Gilardoni, P., Turiel, G., Fan, Z., et al. (2020). Endothelial lactate controls muscle regeneration from ischemia by inducing M2-like macrophage polarization. Cell Metab. *31*, 1136–1153.e7.

49. Qiu, X., Liu, S., Zhang, H., Zhu, B., Su, Y., Zheng, C., Tian, R., Wang, M., Kuang, H., Zhao, X., et al. (2018). Mesenchymal stem cells and extracellular matrix scaffold promote muscle regeneration by synergistically regulating macrophage polarization toward the M2 phenotype. Stem Cell Res. Ther. *9*, 1–15.

50. Dziki, J.L., Wang, D.S., Pineda, C., Sicari, B.M., Rausch, T., and Badylak, S.F. (2017). Solubilized extracellular matrix bioscaffolds derived from diverse source tissues differentially influence macrophage phenotype. J. Biomed. Mater. Res. A *105*, 138–147.

51. Zhu, M., Li, W., Dong, X., Yuan, X., Midgley, A.C., Chang, H., Wang, Y., Wang, H., Wang, K., Ma, P.X., et al. (2019). In vivo engineered extracellular matrix scaffolds with instructive niches for oriented tissue regeneration. Nat. Commun. *10*, 4620.

52. Slivka, P.F., Dearth, C.L., Keane, T.J., Meng, F.W., Medberry, C.J., Riggio, R.T., Reing, J.E., and Badylak, S.F. (2014). Fractionation of an ECM hydrogel into structural and soluble components reveals distinctive roles in regulating macrophage behavior. Biomater. Sci. *2*, 1521–1534.

53. Du, H., Shih, C.-H., Wosczyna, M.N., Mueller, A.A., Cho, J., Aggarwal, A., Rando, T.A., and Feldman, B.J. (2017). Macrophage-released ADAMTS1 promotes muscle stem cell activation. Nat. Commun. *8*, 669.

54. Zhu, H., Zhang, M., Liu, Z., Xing, J., Moriasi, C., Dai, X., and Zou, M.H. (2016). AMP-Activated protein kinase α1 in macrophages promotes collateral remodeling and arteriogenesis in mice in vivo. Arterioscler. Thromb. Vasc. Biol. *36*, 1868–1878.

55. Osses, N., and Brandan, E. (2002). ECM is required for skeletal muscle differentiation independently of muscle regulatory factor expression. Am. J. Physiol. Cell Physiol. *282*, C383–C394.

56. Delaney, K., Kasprzycka, P., Ciemerych, M.A., and Zimowska, M. (2017). The role of TGF-β1 during skeletal muscle regeneration. Cell Biol. Int. *41*, 706–715.

57. Goyal, U., and Ta, M. (2020). A novel role of vitronectin in promoting survival of mesenchymal stem cells under serum deprivation stress. Stem Cell Res. Ther. *11*, 1–14.

58. Ehrig, K., Leivo, I., Argraves, W.S., Ruoslahti, E., and Engvall, E. (1990). Merosin, a tissue-specific basement membrane protein, is a laminin-like protein. Proc. Natl. Acad. Sci. U S A *87*, 3264–3268.

59. Schvartz, I., Seger, D., and Shaltiel, S. (1999). Vitronectin. Int. J. Biochem. Cell Biol. *31*, 539–544.

60. Marchand, M., Monnot, C., Muller, L., and Germain, S. (2019). Extracellular matrix scaffolding in angiogenesis and capillary homeostasis. Semin. Cell Dev. Biol. *89*, 147–156.

61. Stenzel, D., Lundkvist, A., Sauvaget, D., Busse, M., Graupera, M., van der Flier, A., Wijelath, E.S., Murray, J., Sobel, M., Costell, M., et al. (2011). Integrin-dependent and -independent functions of astrocytic fibronectin in retinal angiogenesis. Development *138*, 4451–4463.

62. Sekiya, N., Matsumiya, G., Miyagawa, S., Saito, A., Shimizu, T., Okano, T., Kawaguchi, N., Matsuura, N., and Sawa, Y. (2009). Layered implantation of myoblast sheets attenuates adverse cardiac remodeling of the infarcted heart. J. Thorac. Cardiovasc. Surg. *138*, 985–993.